Development of Advanced Simulation Methods for Solid Earth Simulations

Project Representative
Akira Kageyama The Earth Simulator Center, Japan Agency for Marine-Earth Science and Technology

Authors
Akira Kageyama *1, Mamoru Hyodo *1, Mikito Furuichi *1, Takehiro Miyagoshi *1, Nobuaki Ohno *1, Masanori Kameyama *2 and Kumiko Hori *3

*1 The Earth Simulator Center, Japan Agency for Marine-Earth Science and Technology
*2 Ehime University
*3 Max-Planck-Institut fuer Sonnensystemforschung

We are developing new algorithms and codes for computational solid earth sciences. In the geophysical simulation study, one of the great challenges is to reproduce realistic plate tectonics with mantle convection simulation. We are developing an Eulerian numerical scheme for the steady Stokes flow to solve a deformation of rigid material (plate tectonics) induced by thermal convection of soft fluid (mantle convection). Another important achievement in this fiscal year is high resolution geodyamo simulations based on Yin-Yang grid, using 512 nodes of the Earth Simulator. A new structures of the flow (plume sheets) and electric current field (spring coils) are found in these simulations. We have also developed a new code of earthquake cycle simulations with the elastic/viscoelastic heterogeneity.

Keywords: geodynamo, mantle convection, plate tectonics, ACuTE method, Yin-Yang grid, Eulerian scheme

1. Validity test of a Stokes flow solver by fluid rope coiling: toward plate-mantle simulation

Our simulation scheme combines (i) the multigrid method together with a fast and robust smoother algorithm named ACuTE [1, 2], and (ii) an low diffusive semi-Lagrangian advection algorithm named CIP-CSLR-CS [3]. Since it is easy to optimize in vectorization/parallelization, our method is suitable for large scale simulation.

Last year, we proposed a validity test of our simulation scheme by using a fluid rope coiling event, in which we compared our three dimensional simulation result (3-D model) with a numerical solution of a one dimensional equilibrium problem (1-D model). In this simulation, rigid material is surrounded by a material (called 'air') with small viscosity η_{air} to mimic a free surface of the rope fluid. This year, we summarize results of numerical experiments and show that our simulation scheme can successfully reproduce not only qualitative but also quantitative behavior for a large deformation problem of a curved rigid plate [4] (Fig. 1 and 2).

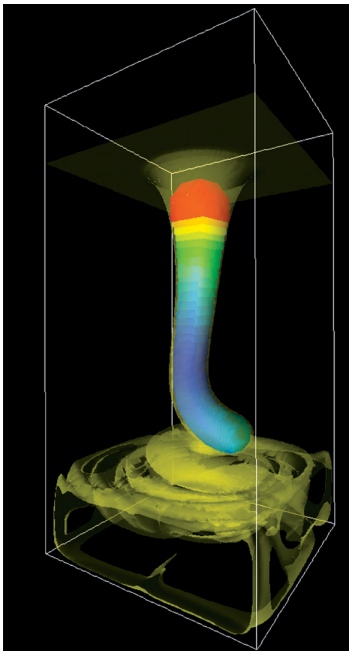

Fig. 1 Results of qualitative comparison for fluid rope properties. Semi-transparent yellow isosurface shows density distribution of rope fluid of 3-D model, and sequence of the colored balls (colored tube) shows solution of 1-D model. Size and color of ball express radius of fluid rope. Agreement of results between our 3-D model and 1-D model are represented by overlaps of isosurface and colored balls.

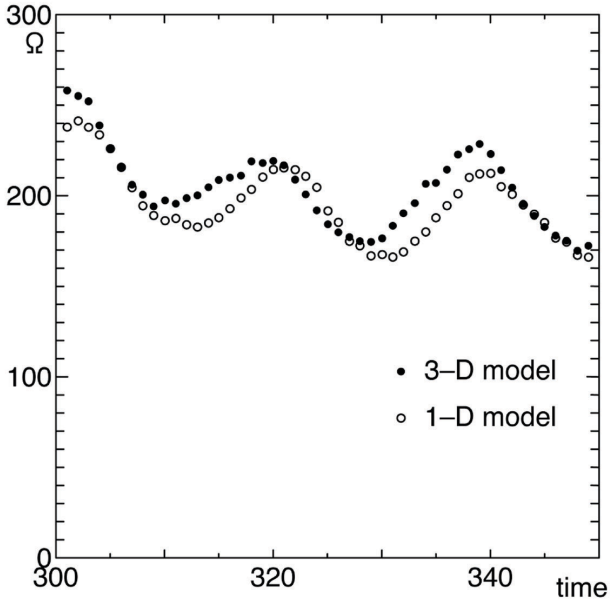

Fig. 2 Results of qualitative comparison for fluid rope properties. Time evolution of angular velocity Ω of fluid rope against vertical axis.

2. Treatment of numerically defined boundary condition

The success of our simulation study for fluid rope coiling event indicates that our approach potentially solves behaviors of numerically defined boundary conditions (e.g. free surface of a rigid plate) of a Stokes flow without serious quantitative errors. We therefore begin to develop a treatment of numerical boundary conditions in a mechanical point of view. This is a step toward plate mantle unified simulation which reproduces a whole Stokes flow motion of the solid earth system.

In this year, we are trying to simulate a self-gravitating motion of the Stokes flow as a free surface problem. It means that a spherical shape, like the real, earth is created in the cubed Cartesian grid. Instead of the previous small viscous air approach, we introduce the stress free condition on an air cell, and we don't have to calculate for the region outside a material (air region). On the other hand, because of the stress free boundary condition and lack of inertial term in a Stokes flow calculation, we have difficulty with the rigid motion of a material since it might devastate the calculation. So we extract such an external force (sometimes due to a desctrization error) that produces the rigid motion of material from the force balance equation. This procedure is also applied to the field of each grid levels of the multigrid algorithm. As a result, we have succeeded in calculating a circular shape from square profile with the fast multigrid iterative manner, even though there is strong viscosity contrast inside the material (Fig. 3).

We also develop a simulation scheme which uses a reproduced sharp plate boundary profile as a brittle breaking plane. We introduce the mechanical boundary conditions, in which a strain rate by the velocity along a brittle plane does not work as the viscous stress. Although many types of treatments for brittle breaking (e.g. yield stress method) are proposed, once brittle breaking occurs, almost all of them just decrease the viscosity on the plate boundaries to represent the breaking situation. On the other hand, our method takes into account the direction of the brittle plane.

3. High Resolution Geodynamo Simulation by Yin-Yang Grid with low Ekman number

In this Fiscal Year, we have done product runs of large scale geodynamo simulations with the Yin-Yang grid [5, 6]. The high performance and parallelization rate of the Yin-Yang grid was already confirmed [7, 8, 9]. We have done geodynamo simulations with low Ekman number. The Ekman number is the ratio of rotation time scale over viscous diffusion time scale. One of the difficulty of geodynamo simulation is that the viscosity of the outer core in the Earth is very low—so Ekman number also becomes very low. The low viscosity requires high resolution simulation. The new geodynamo code with Yin-Yang grid enabled us to

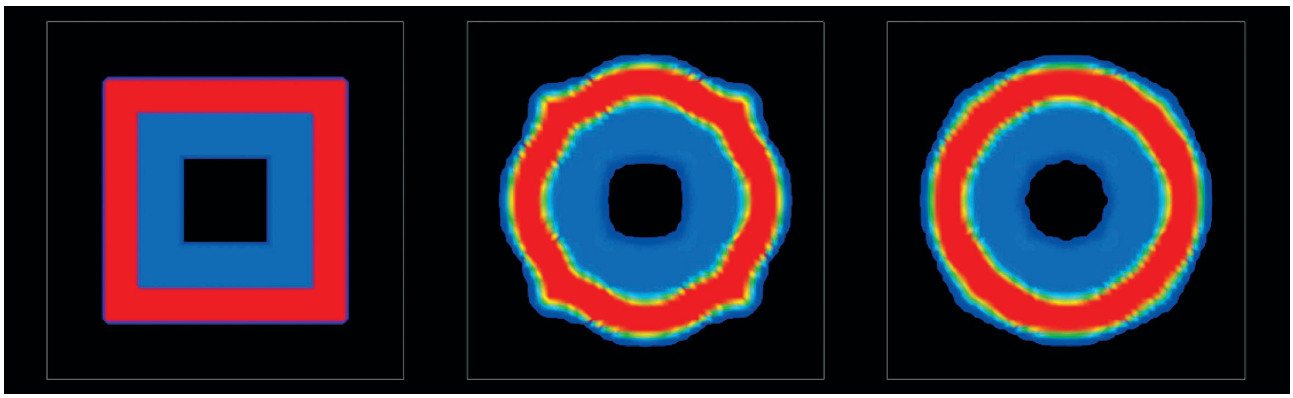

Fig. 3 Time evolution of squared profile in central gravitational field. Viscosity profile is shown by colors: Red means rigid material (η = 1.0) and blue means soft material ($\eta = 10^{-2}$), and black region represents air (no calculation area). Figures show (a) initial state, (b) intermediate state, and (c) final state.

perform high resolution geodynamo simulations on the 4096 processors of the Earth Simulator. The grid size of our simulation is $N_r \times N_\theta \times N_\phi \times 2 = 511 \times 514 \times 1538 \times 2$, where N_r, N_θ, N_ϕ are numbers in radial ($0.3 < r < 1.0$), latitudinal ($\pi/4 < \theta < 3\pi/4$), and longitudinal ($-3\pi/4 < \phi < 3\pi/4$) directions. The last factor × 2 is for *Yin* and *Yang*. Due to this high resolution, we could achieve the Ekman number 2.3×10^{-7}. This is the lowest value achieved to date in geodynamo simulations.

In this low Ekman number regime, the convection, current, and magnetic field structures are quite different from those in higher Ekman numbers which showed formation of positive and negative vorticity columns side by side. Figure 4 shows an overview of the convection structure. Figure 4(a) shows the component along the rotation axis of the vorticity, ω_z, on the equatorial and meridional cross-sections by color contour. The red and blue are for positive and negative vorticity, respectively. The convection is composed of jets in radial direction. The jets are narrow. The peak Fourier mode at $r \sim 0.4$ is about 50. The width of the jets is independent of radius because the jets bifurcate. Figure 4(b) shows a magnified image of the velocity field on the equatorial plane by colored arrows. A part of the inner core is also shown as a spherical mesh. The convection is composed of narrow upstream (toward core-mantle boundary) and downstream (toward inner core) flow. In three-dimension, the convection structure is multiple sheet-like structure elongated in the parallel direction to the rotation axis since the flow structure is almost two-dimensional along the rotational axis by rapidly rotation effect (Taylor-Proudman's theorem). The pattern of ω_z on the meridional cross-section shown in Fig. 4(a) shows this effect well.

Magnetic field is amplified by the magnetohydrodynamic (MHD) dynamo process. The total magnetic energy integrated over the spherical shell region, or the outer core, is several times larger than the convection flow energy. Figure 5(a) shows the radial component of the magnetic field, *Br*. The magnetic fields are bundled. In other words, many magnetic flux tubes are formed. This is also a new discovery in this low Ekman number regime geodynamo. Figure 5(b) shows one of the magnetic flux tube. Magnetic fields are shown by pink tubes. In this figure, current field (blue tubes) and velocity fields (arrows) are also shown. The current structure is helical coil since magnetic flux tubes are formed. The bundled magnetic field is in the helical current coil and is parallel to the axis of the helical current coil. The velocity is also nearly parallel to the magnetic field. This flow is upwelling. We have found that the accelerating upstream flow stretches out the magnetic field lines. Then, the dynamo process, which is conversion of convection kinetic energy to magnetic energy, takes place and magnetic flux tubes are formed there.

Figure 6 shows comparison with other Ekman number case of convection structure. The ω_z on the equatorial plane is shown. Figure 6(a) shows the Ekman number is 2.3×10^{-7} (case a) and Fig. 6(b) shows the case with 2.6×10^{-6} (case b). A remarkable character is the width of the jet. It becomes large in case b. In addition, in case a, magnetic fields in the sheet plumes are almost straight. On the other hand, in case b jets slightly wind to longitudinal direction. Magnetic fields

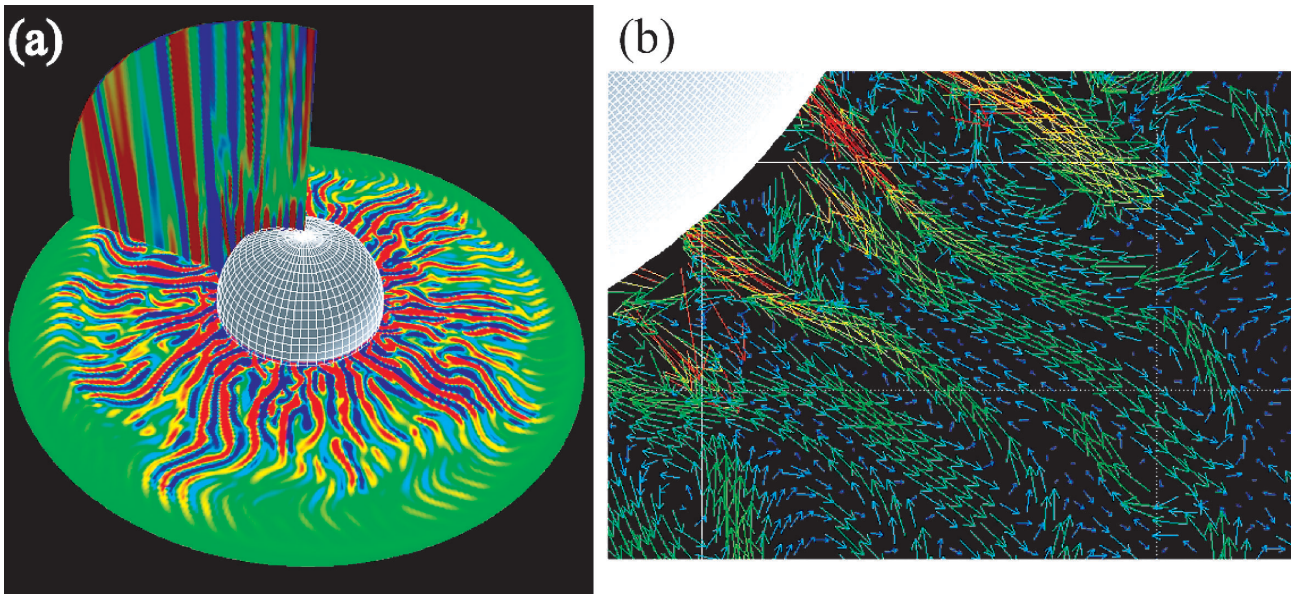

Fig. 4 A high resolution geodynamo simulation using Yin-Yang grid. (a) The component along the rotation axis of the vorticity, ω_z, on the equatorial and meridional cross-sections by color contour. The red and blue is for positive and negative vorticity, respectively. (b) A magnified image of velocity field on the equatorial plane by colored arrows. A part of the inner core is also shown as a spherical mesh.

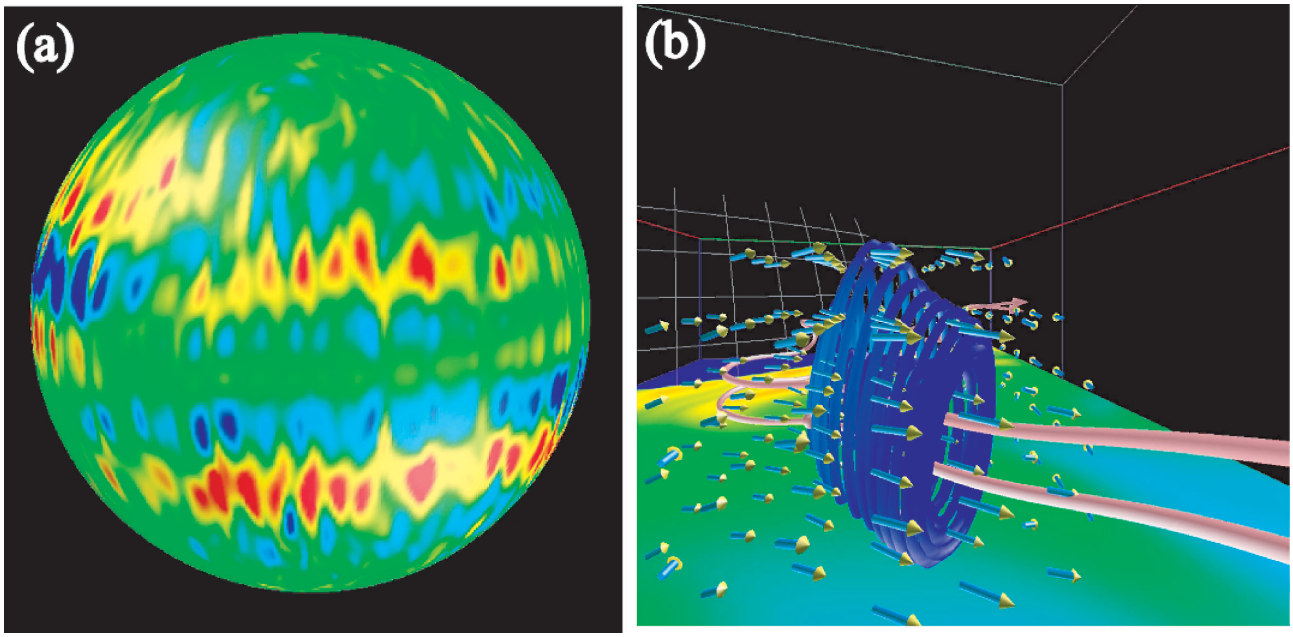

Fig. 5 (a) The radial component of the magnetic field, B_r. Many magnetic flux tubes are formed. (b) A magnified image of one of the magnetic flux tubes. Magnetic fields are shown by pink tubes. Current field (blue tubes) and velocity fields (arrows) are also shown. The current has a helical structure.

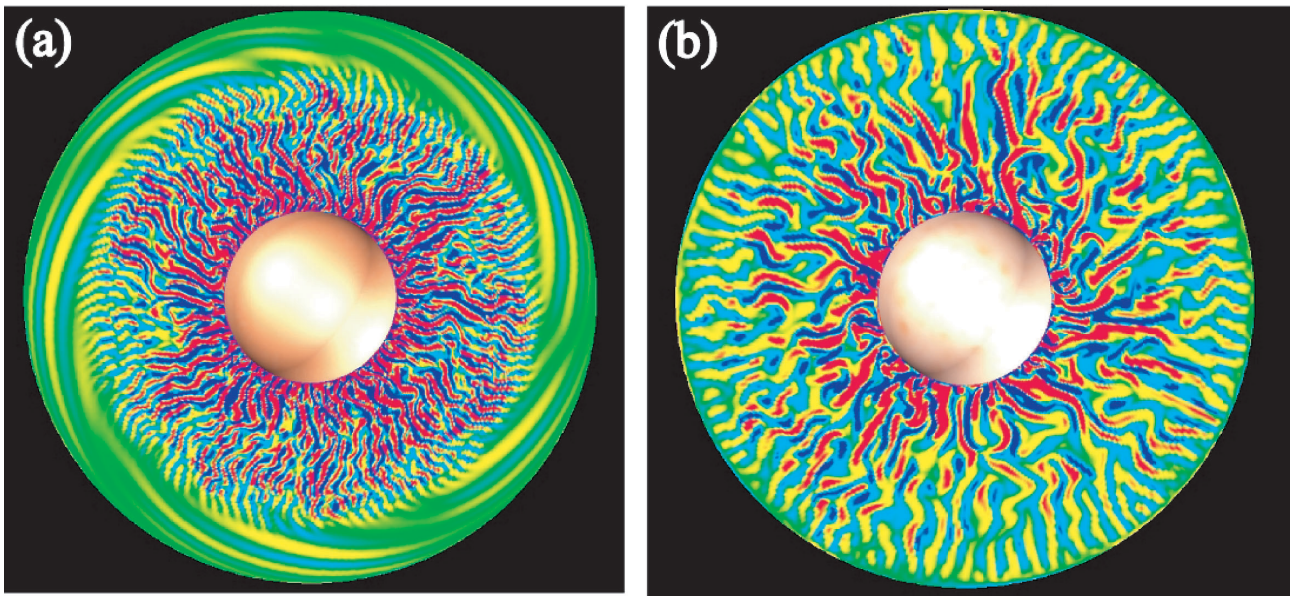

Fig. 6 The vorticity ω_z on the equatorial plane. (a) Ekman number is 2.3×10^{-7}. (b) 2.6×10^{-6}. The width of the jet becomes large in case b.

also wind along the flow. We found in case b, the current coil structure survives, though in a less distinctive fashion.

The new findings in this fiscal year including convection structure (sheet plumes), the current field structure (helical coils), and the magnetic field structure (localized straight flux tubes) are summarized in our recent paper [10].

4. Earthquake cycle simulation

We have developed a new code for 2-D quasi-static earthquake cycle simulations with the elastic/viscoelastic heterogeneity in the material distribution. In many previous quasi-static earthquake cycle simulations which mainly deal with the long-term slow deformation process of earthquake cycle including a quasi-dynamic treatment of dynamic rupture process, the earth is assumed to be purely elastic for the simplicity. Our new code enables us to simulate earthquake cycles under the realistic elastic/viscoelastic structure and complex plate boundary configuration. In FY 2008, we have completed the development of the 2-D simulation code, and performed some numerical simulations of the earthquake

recurrence on dipping faults in the viscoelastic earth model. Among them, we feature results of the simulation which are performed in order to evaluate the effect of the viscoelasticity on earthquake cycles in this report.

As a most simple viscoelastic structure, we constructed a 2-D viscoelastic finite element model consisting of a standard linear solid (SLS) material overlied by an elastic layer with the thickness of 80 km. For numerical stabilization after the viscoelastic relaxation, we use the SLS model in which an elastic spring element with small stiffness is added in parallel to a Maxwell element. We assume the stiffness of the added spring element is assigned to be one percent of the Maxwell element so that the viscoelastic property of SLS is similar to that of Maxwell solid. With homogeneous elastic property in the whole FE model (rigidity :G = 30GPa, Poisson's ratio ν = 0.25), only the effect of the viscosity of SLS on the seismic cycle will be considered in the present calculation. Hereafter, the difference of the viscosity values is represented by a term 'τ_{SLS}' which is defined by the viscosity value of Maxwell element over its rigidity. Following the well-studied plate configuration in elastic simulations, we set an inclined plate boundary with the dip angle of 20°, and assume a rate-and state-dependent friction is acting on the plate interface within the elastic layer. The RS friction includes three frictional parameters A, B and L, which are to be assigned on the plate interface. The parameter A is related to the rate dependence, and the parameters B and L to the frictional surface state. Figure 7 indicates the depth distribution of frictional parameters A and B assumed in this study. The frictional parameter L is the characteristic slip distance during which the friction reaches the new level after the slip rate is changed. In the present simulation, L is assumed to be 25 *cm* independent of depth.

Assuming the relative velocity of plates V_{pl} = 10 *cm/yr*, we perform simulations with several values of τ_{SLS} (3, 10, 30 and ∞ years). In each case of the present simulation for different τ_{SLS}s, the steady aseismic sliding occurs at the deeper part of plate interface, while great earthquakes recur with almost the same interval of 162–164 years at the shallow asperity region of negative *A–B* (see Figure 8). Besides such characteristic similarities, there exist some remarkable differences between simulated earthquake cycles in elastic and viscoelastic earth models. Figure 9 shows the depth distribution of seismic slips and seismic coupling coefficients in simulated earthquake cycles, where we define the seismic slip as the slip distance with a slip velocity higher than 1 cm/s during one earthquake cycle, and the seismic coupling coefficient is the ratio of the seismic slip to total amount of slip during a recurrence interval of great earthquakes. Both the seismic slip and coupling coefficient in the elastic model are larger than those in viscoelastic models. In elastic model, shear loading is caused only by the aseismic sliding just below the seismogenic zone. In viscoelastic case, another shear loading due to the relaxation in SLS material just after the great earthquake continuously prevents the shallow asperity region healing up, hence the degree of stick (i.e. interplate coupling) there is weakened than that of elastic case. As a result of weak interplate coupling throughout the interseismic period, at the preseismic stage, slow pre-slips with velocity slower than 1 cm/*s* need to extend the wider region of the asperity so that the shear stress of the asperity reaches critical state and dynamic slips initiate (note the rela-

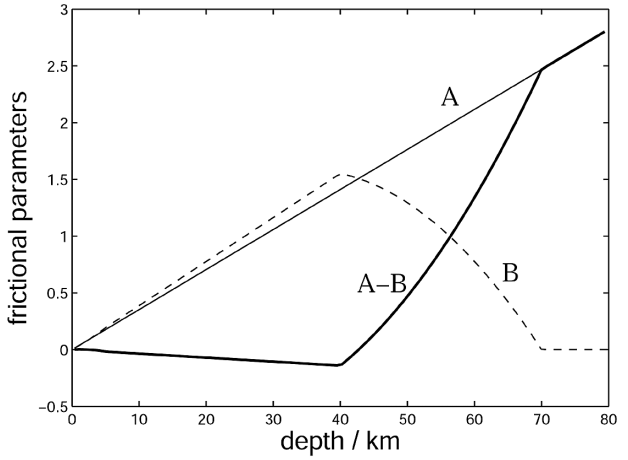

Fig. 7 The depth dependence of frictional constitutive parameters A (thin solid line), B (dotted line), and A-B (thick solid line) assumed in the simulation.

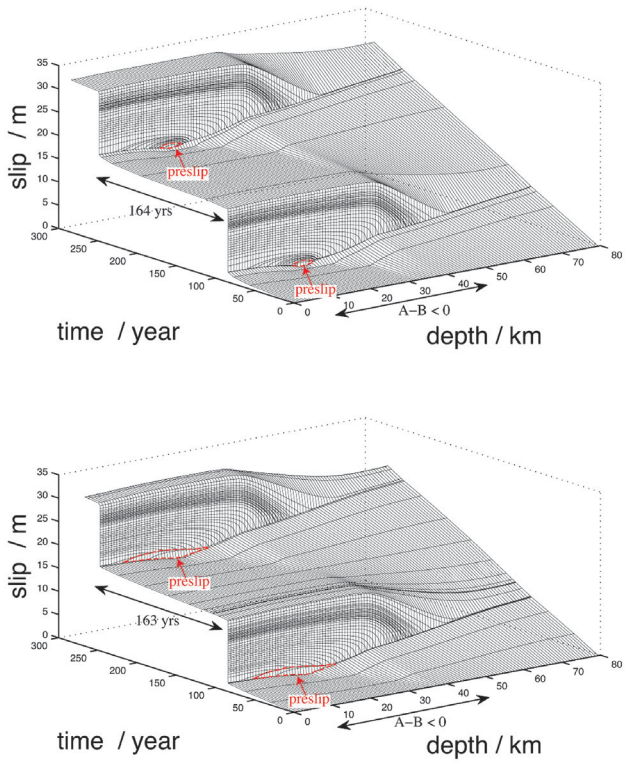

Fig. 8 Spatio-temporal evolution of fault slip on the model plate boundary. (top) elastic model (τ_{SLS} = ∞ years). (bottom) viscoelatic model (τ_{SLS} = 3 years).

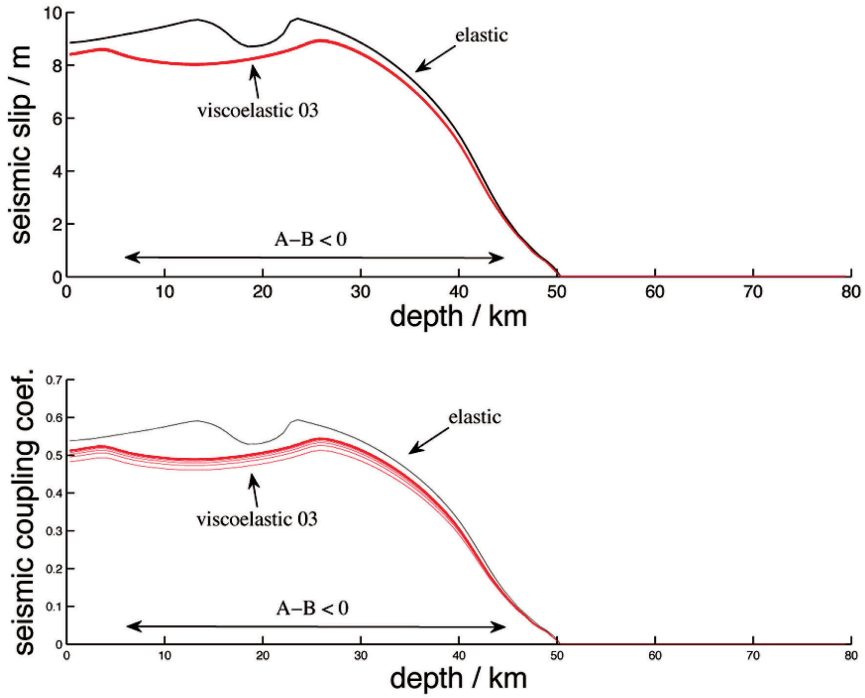

Fig. 9 Depth dependence of (top) the seismic slip and (bottom) seismic coupling coeffient of simulated 15 seismic cycles for elastic and viscoelastic (τ_{SLS} = 3 years) models. In viscoelastic model, the seismic slip has no time dependence, while seismic coupling coefficients (i.e. recurrence intervals) has clear long-term time dependence.

tion between dotted regions in Fig. 8 and cavities of the seismic slip distribution in Fig. 9).

From above results, for dipping faults, it may be concluded that the viscoelasticity largely affects the sliding behaviour on the fault and that the consideration of rheology structures is important for the realistic earthquake cycle simulation.

5. Mantle convection and other topics

Our new simulation code of mantle convection in a spherical shell geometry, combined with the Yin-Yang grid and ACuTE techniques [11], was further applied to the models with solid-state phase transitions. We have successfully reproduced the effects of endothermic post-spinel transition occurring at around 660 km depth from the Earth's surface.

We also studied other topics that are summarized in the following papers: [12, 13, 14, 15, 16, 17].

References

[1] Masanori Kameyama, Akira Kageyama, and Tetsuya Sato. Multigrid iterative algorithm using pseudo-compressibility for three-dimensional mantle convection with strongly variable viscosity, *J. Comput. Phys.*, 206(1):162–181, 2005.

[2] Masanori Kameyama, ACuTEMan: A multigrid-based mantle convection simulation code and its optimization to the Earth Simulator, *J. Earth Simulator*, 4:2–10, 2005.

[3] Mikito Furuichi, Masanori Kameyama, and Akira Kageyama, Three-dimensional Eulerian method for large deformation of viscoelastic fluid: Toward plate-mantle simulation, *J. Comput. Phys.*, 227:4977–4997, 2008.

[4] Mikito Furuichi, Masanori Kameyama, and Akira Kageyama, Validity test of a stokes flow solver by fluid rope coiling: toward plate-mantle simulation, *Phys. Earth Planet. Inter.*, submitted, 2008.

[5] Akira Kageyama and Tetsuya Sato, "Yin-Yang grid": An overset grid in spherical geometry, *Geochem. Geophys. Geosyst.*, 5(9):1–15, 2004.

[6] Akira Kageyama, Dissection of a sphere and Yin-Yang grids, *J. Earth Simulator*, 3:20–28, 2005.

[7] Akira Kageyama, Masanori Kameyama, Satoru Fujihara, Masaki Yoshida, Mamoru Hyodo, and Yoshinori Tsuda, A 15.2 TFlops simulation of geodynamo on the Earth Simulator, *Proceedings of the ACM/IEEE Conference SC2004 (Super Computing 2004)*, ISBN:0-7695-2153-3, pages 35–43, 2004.

[8] Akira Kageyama and Masaki Yoshida, Geodynamo and mantle convection simulations on the earth simulator using the Yin-Yang grid, *J. Physics: Conference Series*, 16:325–338, 2005.

[9] Akira Kageyama, Yin-Yang grid and geodynamo simulation, *Computational Fluid and Solid Mechanics 2005*,

K.J. Bathe (Editor), pages 688–692, 2005.

[10] Akira Kageyama, Takehiro Miyagoshi, and Tetsuya Sato, Formation of current coils in geodynamo simulations, *Nature*, 454:1106–1109, 2008.

[11] Masanori Kameyama, Akira Kageyama, and Tetsuya Sato, Multigrid-based simulation code for mantle convection in spherical shell using Yin-Yang grid, *Phys. Earth Planet. Inter.*, 171:19–32, 2008.

[12] Nobuaki Ohno and Akira Kageyama, Synthesized visualization of vector and scalar fields in CAVE, *Computers and Geosciences*, submitted, 2008.

[13] Kumiko Hori and Shigeo Yoshida, Non-local memory effects of the electromotive force by fluid motion with helicity and two-dimensional periodicity, *Geophys. Astrophys. Fluid Dyn.*, 102(6):601–632, 2008.

[14] Akira Kageyama, Takehiro Miyagoshi, and Nobuaki Ohno, High resolution geodynamo simulation by yin-yang grid and its visualizations, *Proceedings of FCS 2008 (Frontiers of Computational Science 2008), Nagoya*, Oct 2008.

[15] M. Damon, M. Kameyama, M. Knox, D.H. Porter, D.A. Yuen, and E.O.D. Sevre, Interactive visualization of 3D mantle convection, *Visual Geosciences*, 2008.

[16] James B.S.G. Greensky, Wojciech Walter Czech, David A. Yuen, Michael Richard Knox, Megan Rose Damon, Shi Steve Chen, and M. Charley Kameyama, Ubiquitous interactive visualization of 3D mantle convection using a web-portal with Java and Ajax framework, *Visual Geosciences*, 2008.

[17] Masanori Kameyama, Simulation studies of solid earth dynamics on the earth simulator - theoretical backgrounds, tools and outcrops, *International COE of Flow Dynamics Lecture Series, Earth Simulator, Tohoku Univ. Press, Sendai, Japan, S. Maruyama and T. Hashida, editors*, 8:83–125, 2008.

先端的固体地球科学シミュレーションコードの開発

プロジェクト責任者
陰山　聡　海洋研究開発機構　地球シミュレータセンター

著者
陰山　聡*1，兵藤　守*1，古市　幹人*1，宮腰　剛広*1，大野　暢亮*1，亀山　真典*2，堀　久美子*3
*1　海洋研究開発機構　地球シミュレータセンター
*2　愛媛大学
*3　Max-Planck-Institut fuer Sonnensystemforschung

我々の最終的な目標は、地球シミュレータを駆使した大規模計算機シミュレーションを通じて、地球ダイナモとマントル対流をはじめとする地球内部全体の構造とダイナミクスを理解することである。そのために必要となる大規模並列計算手法や基本数値アルゴリズムの独自開発にも積極的に取り組んでいる。

マントル・プレート結合シミュレーションに向けたコード開発：地球シミュレータで行う大規模シミュレーションにおいて、プレートテクトニクスを再現することを目的とし、我々は連続体としての性質が大きく異なる、マントルとプレートを同時に扱うシミュレーション手法を開発している。本年度は、まず前年度に開発したfluid rope coiling現象を用いた大変形問題に対する新しいベンチマークテストを行った。さらに脆性破壊や、マントルの熱対流の結果として現れるプレート表層の変形などを、力学モデルとして取り扱うための手法の拡張に新たな取り組みを始めた。

地球ダイナモシミュレーション：本年度は、前年度までに開発したインヤン格子を用いた地球ダイナモシミュレーションコードを用いてプロダクトランを行った。コードの高い並列化性能の為、地球シミュレーターの4096プロセッサを用いて非常に高い解像度（約8億格子点）の地球ダイナモシミュレーションを行うことができた。そのためエクマン数をO(10E-07)の領域まで下げることができた。その結果、この領域における対流構造やダイナモ機構は、高いエクマン数領域のものとは大きく異なる事が分かった。対流は、50本以上の上昇および下降するシート状プルームから成り、さらにそれは半径方向に枝分かれする。プルームの幅はどこでもほぼ一定になる。磁場は局所的に束ねられ、磁束管が形成されることが分かった。その結果、電流構造は磁束管を取り巻くヘリカルコイル構造となることも分かった。このような磁束管は上昇プルームに沿って形成されやすく、上昇プルームが磁場を引き伸ばしダイナモ作用が起こり、磁束管が形成される事が分かった。エクマン数を約10倍大きく変化させると、プルームの幅が太くなることが分かった。また流れに蛇行する部分が見られるようになり、それに伴って蛇行する磁場も見られるようになった。ヘリカルコイル電流構造はおおむね維持されるが、やや崩れた構造になる。

地震サイクルシミュレーション：プレート沈み込みに伴う巨大地震の断層面への応力蓄積、そこでの地震発生による応力解放といったプレート境界で発生する一連のプロセスを計算機上で再現する試みは、地震サイクルシミュレーションと呼ばれる。先行研究では、媒質として、「ずれ」に対する応力応答の解析関数が分かっている均質半無限弾性媒質のような理想化媒質を仮定し、断層にわたる「ずれ」と「ずれ応答」との積の境界積分によって応力場を精度よく評価している。しかし、日本列島のような沈み込み帯では、地震波トモグラフィーから示唆される強い不均質構造が存在する。こういった解析的には「ずれ応答」が求まらない複雑な不均質構造を考慮し、その影響をシミュレーションに反映させることが、現実的なシミュレーションを実行するために不可欠である。つまり、1）断層近傍の応力場を精度良く評価すること、2）不均質弾性・粘弾性媒質の取り扱いが可能であること、の両者を満足する計算手法が必要となるが、境界積分方程式法・有限要素法などの単一の数値計算手法では、これらの両立は困難である。このため、両手法の長所のみを抽出・カップルさせる手法を開発し、有限要素法ベースの2次元地震サイクルシミュレーションコードに実装して、その有効性を検証した。境界積分方程式法とのカップリングにより断層近傍で極端に細かなメッシュを使用することなく精度の良い2次元粘弾性不均質場での地震サイクル計算が可能となった。

キーワード：地球ダイナモ, マントル対流, ACuTE法, インヤン格子, 粘弾性流体, 地震サイクルシミュレーション